Intrinsic structural distortion and superexchange interaction in the orthorhombic rare-earth perovskites RCrO$_3$

J.-S. Zhou,[1,*] J. A. Alonso,[2] V. Pomjakushin,[3] J. B. Goodenough,[1] Y. Ren,[4] J.-Q. Yan,[5] and J.-G. Cheng[1]

[1]*Texas Materials Institute, University of Texas at Austin, Austin, Texas 78712, USA*
[2]*Instituto de Ciencia de Materiales de Madrid, CSIC, Cantoblanco, E-28049 Madrid, Spain*
[3]*Laboratory for Neutron Scattering, Paul Scherrer Institut, ETH Zurich, CH-5232 Villigen PSI, Switzerland*
[4]*Advanced Photon Source, Argonne National Laboratory, Argonne, Illinois 60439, USA*
[5]*Division of Materials Science and Engineering, Ames Laboratory, Ames, Iowa 50011, USA*

High-resolution neutron powder diffraction has been applied to determine the structural evolution in the orthorhombic perovskite RCrO$_3$ family. The structural distortions observed have been found to be closely related to the dramatic variation in the magnetic ordering temperature T_N. In addition to the reduction in the orbital overlap integral that can account for the change in T_N in the RFeO$_3$ family, the effect of t-e hybridization due to the structural distortions are responsible for the dramatic change in T_N across the RCrO$_3$ family.

I. INTRODUCTION

The magnetic properties of RCrO$_3$ are extensively reported in three consecutive reviews of perovskite oxides that cover a huge number of studies over a half century.[1] The magnetic structure of the orthochromites was also well-studied during the boom of neutron diffraction in 1960s–1970s. All kinds of magnetic structure in the orthorhombic perovskites can be well-described in connection with the crystal symmetry under the notation developed by Bertaut.[2] In most cases, the collinearly ordered spins are along the a or c axis of the *Pbnm* cell. However, the coupling between the magnetic moment on the rare earth and the spins on Cr^{3+} is responsible for an easy-axis rotation below T_N in some orthochromites.[3] Since the T_N of RCrO$_3$ changes monotonically from Lu to La independent of the rare-earth moment, the R-O-Cr coupling appears to have negligible influence on the Cr-O-Cr coupling. It has been widely accepted that the M-O-M bond angle (M=transition metal), which is reduced from 180° due to the cooperative octahedral-site rotations in the orthorhombic perovskite, is a major factor entering the perturbation formula $J \sim b^2/U$ of the M-O-M superexchange interaction; b is the orbital overlap integral over the M-O-M bond and U is the on-site Coulomb energy. This assumption has been shown to work properly in RFeO$_3$.[4] In contrast, all Jahn-Teller (JT) active systems, such as RTiO$_3$,[5,6] RVO$_3$,[7,8] and RMnO$_3$,[9] do not show a clear connection between the magnetic transition temperatures and the M-O-M bond angle. Instead, they exhibit transitions between different types of spin orderings as the rare earth R changes from La to Lu. As in RFeO$_3$, orbital ordering is not an issue in RCrO$_3$; both families exhibit the type-G spin ordering. Given the same superexchange coupling parameter J in the formula $k_B T_N = 4S(S+1)J$, a huge difference between $T_N=760$ K in LaFeO$_3$ and $T_N=298$ K in LaCrO$_3$ can be well accounted for by the total spin $S=5/2$ for Fe^{3+}:$t^3 e^2$ and $S=3/2$ for Cr:$t^3 e^0$. However, a dramatic change in T_N from LaCrO$_3$ to LuCrO$_3$ appears troublesome for applying the same overlap integral reduction as in RFeO$_3$. Due to incomplete structural data, no attempt has been made so far to answer whether the M-O-M bond-angle evolution over R^{3+} ion can justify the

change in Néel temperature in the RCrO$_3$ family. In this paper, we report results of high-resolution neutron diffraction on all RCrO$_3$ members except a few neutron-absorbing rare earths. By comparison with the structural work of the RFeO$_3$ family in the literature, we are able to identify the local structural distortion that is intrinsic to the orthorhombic perovskite. We have shown that the scenario of overlap integral versus T_N, which has been assumed to be generally applicable in the superexchange interaction, is limited to some special cases like in RFeO$_3$ where both t and e orbitals are half filled. The observed overall change in T_N across the RCrO$_3$ family can be explained well only after the effect of t-e hybridization due to the local site distortion and cooperative octahedral-site rotation is taken into account.

II. EXPERIMENT

Polycrystalline samples of RCrO$_3$ were prepared by standard solid-state reactions. The mixtures of rare-earth oxides and chromium oxide in a stoichimetric ratio were sintered in air at 980–1450 °C with several intermediate grindings. We prepared about 7 g of powder sample for each member in the RCrO$_3$ family to ensure high quality neutron-diffraction data. These materials were checked to be single phase by x-ray powder diffraction (XRD). Neutron powder-diffraction (NPD) patterns were collected at the high-resolution powder diffractometer (HRPT) (Ref. 10) of the SINQ spallation source at the Paul Scherrer Institute, Villigen, Switzerland. The samples were packed in cylindrical vanadium holders of 6 mm diameter excepting the DyCrO$_3$, which was contained in a double-walled sample holder to minimize neutron absorption. The patterns were collected at room temperature with a wavelength of 1.494 Å. In all cases the high-intensity mode was used; the collection time was about 4 h per diagram (20 h for DyCrO$_3$). The NPD patterns were analyzed with the Rietveld method with the FULLPROF (Ref. 11) program. The magnetization measurements were carried out in a superconductor quantum interference device magnetometer (Quantum Design). All crystal-structure and magnetization data will be published separately. We present here our major results.
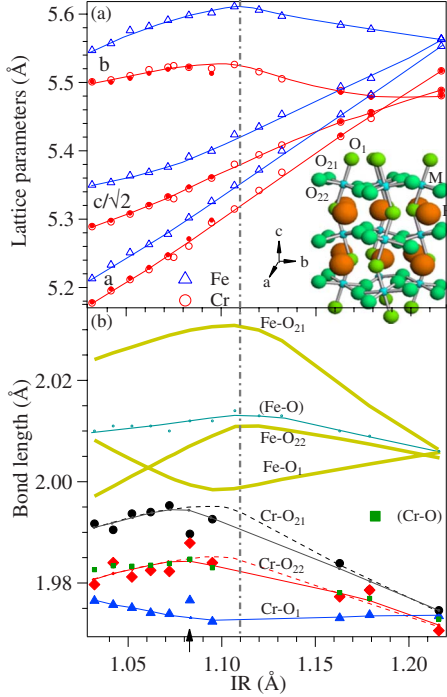
FIG. 1. (Color online) The IR dependences crossing all rare-earth ions from Lu^{3+} to La^{3+} of (a) lattice parameters (solid symbols are from neutron diffraction) and (b) M-O bond lengths of $RCrO_3$. Error bars are comparable to the size of symbols. The anomalous bond lengths of $DyCrO_3$, shown by an arrow, are attributed to the Dy neutron absorption. The inset shows the structural model of the *Pbnm* perovskite.

III. RESULTS AND DISCUSSION

A precise knowledge of the crystal structure is always essential for interpretation of the physical properties. We first made a thorough analysis of the crystal structure of $RCrO_3$ in comparison with that of $RFeO_3$ since the latter is a model system in which the T_N variation can be well accounted for by the M-O-M bond angle. We start by analyzing the lattice parameters of $RCrO_3$ and $RFeO_3$ as a function of the ionic radius (IR) of the R^{3+} ions, Fig. 1(a). The lattice parameters in both systems show the same trend as IR increases. Major features include (1) $b > c/\sqrt{2} > a$ for most R as required by the crystal symmetry of the *Pbnm* space group provided that the octahedra are rigid and (2) the curve b versus IR shows an anomaly near IR = 1.11 Å in contrast to the straight line predicted by the software SPUDS (Ref. 12) for rigid octahedra. The anomaly in feature (2) is universal for all the ortho-rhombic perovskites[13] as the O_{21}-M-O_{22} bond angle shown in Fig. 2(a) starts to decrease from 90° for IR > 1.11 Å. The resulting decrease in the rotation b axis leads eventually to a $b < a$ as is seen in $LaCrO_3$. As a general character of the *Pbnm* perovskites, the long M-O bond is always within the ab plane. The Fe-O_{21} and Fe-O_{22} bond lengths reach their maximum near IR = 1.11 Å; at the same IR, the apical Fe-O_1 is located at a minimum. Although no data are available for the $RCrO_3$ with the neutron absorbers R = Sm, Eu, and Gd, we have good reasons to believe that bond lengths versus IR follow the dashed lines in Fig. 1(b) similar to that of $RFeO_3$

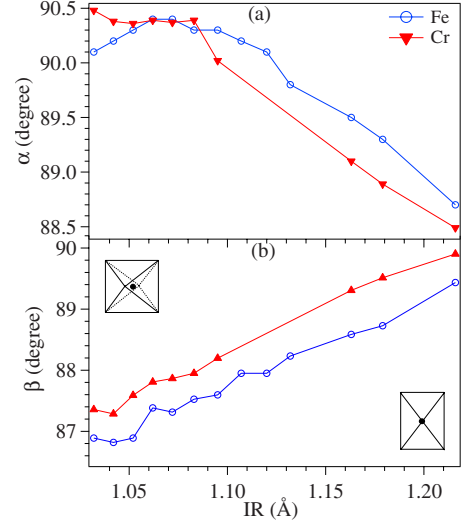FIG. 2. (Color online) The IR(R^{3+}) dependence of (a) the O_{21}-M-O_{22} bond angle α and (b) the angle β between M-O_1 bond and the O_{21}-M-O_{22} plane. Insets: octahedron projected along the axis normal to the O_{21}-M-O_{22} plane.

since they all share the same features of lattice parameters. The largest bond-length splitting in both systems occurs near IR = 1.11 Å. The classic case of $RFeO_3$ was accomplished by using x-ray single-crystal diffraction[14] in which the Fe-O bond lengths were determined within large error bars. We have reproduced here in Fig. 1(b) the guide lines that go through scattered data points of the Fe-O bond lengths versus IR in $RFeO_3$.[14] The results of our NPD data trace down the profile of Cr-O bonds as a function of IR with high precision. Since there is no orbital order to have an influence on the magnetic interactions in these two JT-inactive systems, we focus on the superexchange interaction that is modulated by structural distortions.

We turn to the Cr-O-Cr bond angle, the so-called "super-exchange angle" in the orthorhombic perovskites. As shown in Fig. 3(a), the averaged Cr-O-Cr bond angle θ is progressively reduced from 180° as the IR decreases. As a matter of fact, the profile of θ versus IR is nearly identical in several orthorhombic perovskites RMO_3 (M = Ti, V, Cr, Mn, Fe, Ga). For a given R, $RCrO_3$ has the smallest octahedral-site tilting angle among these perovskite families because of the relatively smaller bond-valence-sum radius of the Cr^{3+} ion and therefore larger geometric tolerance factor t. Without a rigorous proof so far, the empirical relationship between the superexchange coupling J and the superexchange angle for the $RFeO_3$ family has undergone an evolution from $J \sim \cos \theta$ (Ref. 15) to $J \sim \cos^2 \theta$ (Ref. 16) and finally to $J \sim \cos^4(\omega/2)/d^7$ (Ref. 4), where d denotes the M-O bond length and $\omega = 180 - \theta$. As shown in Fig. 1(b), d is essentially independent of IR for $RFeO_3$ and can be taken as an averaged bond length. In order to make a quantitative comparison of the calculated T_N based on the structural data and the observed T_N, we have normalized T_N by that of $LaMO_3$. The calculation based on the formula $J \sim \cos^4(\omega/2)/d^7$ can indeed produce the essential feature of the observed T_N versus IR for the $RFeO_3$ family in Fig. 3(b). However, this angle dependence can only account for about 30% of the overall
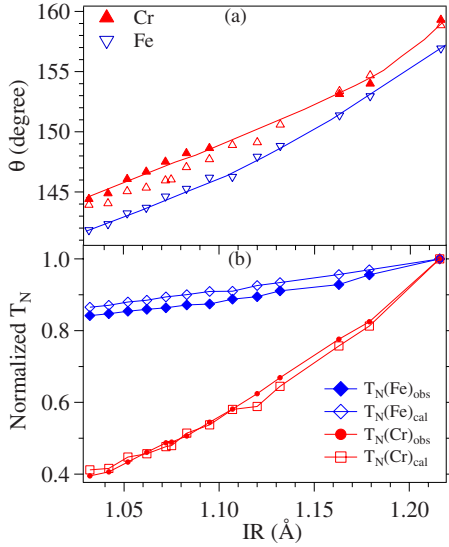
FIG. 3. (Color online) The IR(R^{3+}) dependences of (a) the averaged M-O-M bond angle θ (hollow symbols are from XRD) and (b) normalized T_N of RFeO$_3$ and RCrO$_3$ by $T_N = 740$ K for LaFeO$_3$ and 289 K for LaCrO$_3$, respectively. T_N of RFeO$_3$ are after Ref. 15.

change in T_N across the RCrO$_3$ family. Some important spin-spin interaction term in addition to the change in the super-exchange angle is missing in our understanding of the RCrO$_3$ family.

What has been ignored is the hybridization between inter-site t-e orbitals which are orthogonal for a 180° M-O-M bond. As illustrated in Fig. 4, octahedral-site tilting not only reduces the t orbital overlap integral considered but also introduces the orbital overlap between the π and the σ bonds. The influence on the overall exchange interaction of the intersite t-e orbital hybridization is sharply different for Fe^{3+}:$t^3 e^2$ versus Cr:$t^3 e^0$. The superexchange interaction between two adjacent transition-metal ions is delivered by a virtual charge transfer (VCT). Figure 5 illustrates the case for
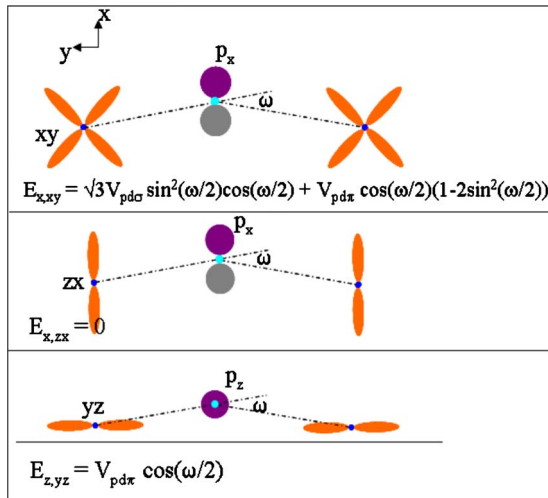

FIG. 4. (Color online) Schematic diagram of orbital overlap integrals. These are the examples of 15 two-center orbital overlap integrals. Formulas inside diagram show the angle dependence of the overlap integral. See text for the bond-length dependence V_{pd}.
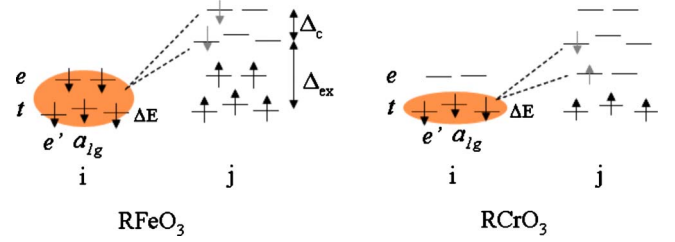

FIG. 5. (Color online) Schematic diagram of the hybridization effect on the virtual charge transfer for the superexchange interaction in perovskites RCrO$_3$ and RFeO$_3$. The VCT occurs for all occupied spin states; only those for the representative magnetic couplings are shown in the figure. Δ_c stands for the crystal-field splitting, Δ_{ex} is the exchange splitting, $\Delta E = E_{a1g} - E_e$.

the Fe^{3+} ions. The superexchange interactions over the half-filled π bond t^3-O-t^3 and the half-filled σ bond e^2-O-e^2 are all antiferromagnetic (AF) according to the superexchange rules. The t-e hybridization does not bring in any new component to the overall superexchange interaction in this case. The reduction in the σ bond overlap integral b^σ due to octahedral-site rotation appears not to be compensated by a small gain of the overlap integral through the intersite t-e hybridization. Therefore, the angular dependence of J $\sim \cos^4(\omega/2)/d^7$, which considers only the σ bond, is still a good approximation. In the case of RCrO$_3$, however, only the t orbitals are half filled. A t-e hybridization similar to that in RFeO$_3$ introduces a VCT to the empty e component of the hybridized orbital at site j, i.e., t^3-O-e^0, which leads to a ferromagnetic coupling J_{hb}^σ according to the superexchange rules. The cartoon for RCrO$_3$ in Fig. 5 shows the t-e hybridization that leads to the ferromagnetic VCT to the empty e orbital on site j whereas the t^3-O-t^3 transfer gives a dominant AF coupling J^π. The final superexchange interaction for the type G antiferromagnetic ordering is $J = J^\pi - J_{hb}^\sigma$. The progressively enhanced J_{hb}^σ becomes comparable to the angle-θ-dependent J^π as IR decreases. In order to check whether this argument can account quantitatively for the observed T_N versus IR, we have derived J^π and J_{hb}^σ by including all possible two-center orbital overlap integrations between (p_x, p_y, p_z) on O^{2-} and $(xy, yz, zx, x^2-y^2, z^2-r^2)$ on Cr^{3+} based on the Slater-Koster tables of interatomic matrix elements,[17] which gives the following angle dependence for the orbital overlap integrals b^π and b_{hb}^σ

$$b_{hb}^\sigma = [\cos(\omega/2) + \sin(\omega/2)] \left\{ \sqrt{3} \cos(\omega/2)\sin(\omega/2) \right.$$
$$\left. + \frac{\sqrt{3}}{2}[\cos^2(\omega/2) - \sin^2(\omega/2)] - \frac{1}{2} \right\} V_{pd\sigma},$$

$$b^\pi = \{2[\sin(\omega/2) + \cos(\omega/2)] - 4\sin(\omega/2)\cos^2(\omega/2)\} V_{pd\pi}.$$

Therefore, the superexchange coupling J can be expressed by

$$J = J_0[(b^\pi)^2 - \eta(b_{hb}^\sigma)^2], \quad \eta = \frac{U + \Delta_{ex}}{U + \Delta_c}\left(\frac{V_{pd\sigma}}{V_{pd\pi}}\right)^2.$$

J_0 here is a constant that determines the absolute value of T_N but it has no effect on the calculation of a normalized T_N in

Fig. 3(b). A match between the observed T_N and the calculated value like that shown in Fig. 3(b) requires an $\eta = 1.5$. That is a highly reasonable number since the bond-length-dependent integral $V_{pd\sigma}$ is slightly larger than $V_{pd\pi}$ in oxides as has been shown by Harrison[18] and Δ_{ex} is slightly larger than Δ_c in octahedral-site Cr^{3+}.

Another local site distortion is the angle β between the apical M-O_1 bond and the O_{21}-M-O_{22} plane. As seen from Fig. 2(b), this angle is near 90° for $LaFeO_3$ but it is reduced monotonically as IR decreases. The same angle change can also be seen in $RCrO_3$. Landron and Lepetit[19] have shown that the intrasite hybridization between t and e orbitals is highly sensitive to the angle β (they have defined the trigonal distortion of an octahedron by a different angle). In our case, the intrasite t-e hybridization vanishes for $\beta = 90°$. The component of e orbital mixing into the t orbital due to the trigonal distortion of the octahedral site is extremely small in our case but the intrasite hybridization splits the degenerated t_2 orbitals into $2 \times e'$ and a_{1g}. The intrasite hybridization strengthens the ferromagnetic coupling $J_{hb}^{\sigma} = (b_{hb}^{\sigma})^2/(U + \Delta_c)$ by offsetting a $\Delta E = E_{e'} - E_{a1g}$ in the energy difference $U + \Delta_c$ associated with this VCT.

The intersite t-e hybridization should influence physical properties in all orthorhombic perovskites. The $RCrO_3$ family with $t^3 e^0$ exemplifies clearly the effect. The same mechanism should also be applicable to another system with $t^3 e^0$, for example, the perovskites $AMn^{4+}O_3$ (A = Ca, Sr, and $Sr_{1-x}Ba_x$) (Ref. 20) where T_N is found to be very sensitive, though less dramatically than that in $RCrO_3$, to IR. However, other factors such as the size variance and the change in A-O covalency have to be included in order to account for the curve of T_N versus IR quantitatively in the $AM^{4+}O_3$ perovskites. In the JT-active family $RTiO_3$, orbitals remain disordered in the paramagnetic phase. Fitting to a Curie-Weiss law of the paramagnetic susceptibility gives an antiferromagnetic coupling for the $RTiO_3$ family with larger IR and a ferromagnetic coupling for those with smaller IR. The intrinsic local site distortions are certainly playing a role for the transition of the magnetic interaction by confining orbital fluctuations in such a way that the AF t^1-O-t^1 coupling is preferred for the $RTiO_3$ with large IR and the ferromagnetic t^1-O-t^0 for those with smaller IR. However, long-range magnetic order and orbital order occur at the same temperature,[6] which indicates that orbital order is a prerequisite to long-range magnetic order. The increasing ferromagnetic t^1-O-e^0 coupling as IR decreases contributes to the transition from the antiferromagnetic phase to the ferromagnetic phase shown in the phase diagram of the $RTiO_3$ family.[5] In another JT-active family, RVO_3, the orbital flipping transition in the magnetically ordered phase occurring for $IR \leq r_{Dy}$ cannot be explained only by the change in geometric tolerance factor t.

A careful comparison between the effects of hydrostatic pressure versus uniaxial pressure has clarified the effect to be due to the t-e hybridization in these highly distorted perovskites.[21]

IV. CONCLUSION

The structural evolution of orthorhombic $RCrO_3$ has been resolved by high-resolution neutron diffraction. A side-by-side comparison with that of $RFeO_3$ gives a solid proof that the following local structural distortions are intrinsic to orthorhombic perovskites RMO_3: (a) the longest M-O bond length is within the O_{21}-M-O_{22} plane, (b) the bond-length splitting undergoes a maximum at a middle IR near 1.11 Å, (c) at the same IR the O_{21}-M-O_{22} bond angle α starts to deviate from 90°, and (d) the angle β between the apical M-O_1 bond and the O_{21}-M-O_{22} plane, which is near 90° for $LaFeO_3$ and $LaCrO_3$, reduces monotonically as IR decreases. These intrinsic structural distortions are in addition to the cooperative octahedral-site rotations, widely called the $GdFeO_3$-type distortion, and are essential elements to interpret physical properties in these perovskites. As a consequence of structural distortions that include the cooperative octahedral-site rotation and local distortions, the t-e hybridization is inevitable. For $RFeO_3$, where the AF coupling consists of the superexchange interactions of the t^3-O-t^3 and e^2-O-e^2 orbitals, the hybridization does not bring any new component. Therefore the empirical angle dependence of the superexchange coupling J remains a good approximation. The more dramatic change in T_N in the $RCrO_3$ family highlights the importance of the t-e hybridization effect. The ferromagnetic coupling through the superexchange interaction t^3-O-e^0 is comparable to the antiferromagnetic coupling through the superexchange interaction t^3-O-t^3. By considering all possible two-center orbital overlap integrals involved in the virtual charge transfer for the superexchange interaction in the orthorhombic perovskite structure, we are able to account quantitatively for the observed T_N versus IR in the $RCrO_3$ family.

ACKNOWLEDGMENTS

*jszhou@mail.utexas.edu

[1] J. B. Goodenough and J. M. Longo, *Crystallographic and magnetic properties of perovskite and perovskite-related compounds*, Landolt-Bornstein, New Series, Group III Vol. 4, Pt. A (Springer-Verlag, Berlin, 1970), p. 126; K. Enke, J. Fleischhauer, W. Gunber, P. Hansen, S. Nomura, W. Tolksdorf, G. Winkler, and U. Wolfmeier, *Magnetic and other properties of oxides and related compounds*, Landolt-Bornstein, New Series, Group III Vol. 12 (Springer-Verlag, Berlin, 1978), p. 368; Y. Endoh, K. Kakurai, A. K. Katori, M. S. Seehra, G. Srinivasan, and H. P. J. Wijn, *Magnetic properties of non-metallic inorganic compounds based on transition elements, Subvolume f3, Perovskites II, Oxides with Corundum, Ilmenite and Amorphous Structures*, Landolt-Bornstein, New Series, Group III Vol. 27 (Springer-Verlag, Berlin, 1994), p. 1.

[2] E. F. Bertaut, in *Magnetism*, edited by G. T. Rado and H. Suhl (Academic Press, New York, 1963), Vol. 3, p. 149.

[3] R. M. Hornreich, J. Magn. Magn. Mater. **7**, 280 (1978).

[4] J.-S. Zhou and J. B. Goodenough, Phys. Rev. B **77**, 132104 (2008).

[5] A. C. Komarek, H. Roth, M. Cwik, W.-D. Stein, J. Baier, M. Kriener, F. Bouree, T. Lorenz, and M. Braden, Phys. Rev. B **75**, 224402 (2007).

[6] J.-G. Cheng, Y. Sui, J.-S. Zhou, J. B. Goodenough, and W. H. Su, Phys. Rev. Lett. **101**, 087205 (2008).

[7] J.-S. Zhou, J. B. Goodenough, J.-Q. Yan, and Y. Ren, Phys. Rev. Lett. **99**, 156401 (2007).

[8] J.-Q. Yan, J.-S. Zhou, J. B. Goodenough, Y. Ren, J.-G. Cheng, S. Chang, J. Zarestky, O. Garlea, A. Llobet, H. D. Zhou, Y. Sui, W. H. Su, and R. J. McQueeney, Phys. Rev. Lett. **99**, 197201 (2007).

[9] J.-S. Zhou and J. B. Goodenough, Phys. Rev. Lett. **96**, 247202 (2006).

[10] P. Fischer, G. Frey, M. Koch, M. Konnecke, V. Pomjakushin, J. Schefer, R. Thut, N. Schlumpf, R. Burge, U. Greuter, S. Bondt, and E. Berruyer, Physica B **276-278**, 146 (2000).

[11] J. Rodriguez-Carvajal, Physica B **192**, 55 (1993).

[12] M. W. Lufaso and P. M. Woodward, Acta Crystallogr., Sect. B: Struct. Sci. **57**, 725 (2001).

[13] J.-S. Zhou and J. B. Goodenough, Phys. Rev. Lett. **94**, 065501 (2005).

[14] M. Marezio and P. D. Dernier, Mater. Res. Bull. **6**, 23 (1971); M. Marezio, J. P. Remeika, and P. D. Dernier, Acta Crystallogr., Sect. B: Struct. Crystallogr. Cryst. Chem. **26**, 2008 (1970).

[15] D. Treves, M. Eibschutz, and P. Coppens, Phys. Lett. **18**, 216 (1965); M. Eibschütz, and D. Treves, Phys. Rev. **156**, 562 (1967).

[16] C. Boekema, F. van der Woude, and G. A. Sawatzky, Int. J. Magn. **3**, 341 (1972).

[17] J. C. Slater and G. F. Koster, Phys. Rev. **94**, 1498 (1954).

[18] W. A. Harrison, *Elementary Electronic Structure* (World Scientific, New Jersey, 2004), pp. 646, 693–703.

[19] S. Landron and M.-B. Lepetit, Phys. Rev. B **77**, 125106 (2008).

[20] O. Chmaissem, B. Dabrowski, S. Kolesnik, J. Mais, D. E. Brown, R. Kruk, P. Prior, B. Pyles, and J. D. Jorgensen, Phys. Rev. B **64**, 134412 (2001).

[21] J.-S. Zhou, J. B. Goodenough, J.-Q. Yan, J.-G. Cheng, K. Matsubayashi, Y. Uwatoko, and Y. Ren, Phys. Rev. B **80**, 224422 (2009).